KeAi
CHINESE ROOTS
GLOBAL IMPACT

Available online at www.sciencedirect.com

ScienceDirect

Green Energy & Environment 9 (2024) 713–722

www.keaipublishing.com/gee

Research paper

Pairing nitroxyl radical and phenazine with electron-withdrawing/-donating substituents in "water-in-ionic liquid" for high-voltage aqueous redox flow batteries

Zhifeng Huang [a,b,*], Rolf Hempelmann [a], Yiqiong Zhang [c], Li Tao [b,*], Ruiyong Chen [a,d,*]

[a] Transfercenter Sustainable Electrochemistry, Saarland University and KIST Europe, 66125, Saarbrücken, Germany
[b] State Key Laboratory of Chem/Bio-Sensing and Chemometrics College of Chemistry and Chemical Engineering Hunan University, Changsha, 410082, Hunan, China
[c] College of Materials Science and Engineering Changsha University of Science and Technology, Changsha, 410114, Hunan, China
[d] Materials Innovation Factory, Department of Chemistry, University of Liverpool, Liverpool, L69 7ZD, United Kingdom

Received 14 July 2022; revised 6 September 2022; accepted 13 September 2022
Available online 17 September 2022

Abstract

Aqueous redox-active organic materials-base electrolytes are sustainable alternatives to vanadium-based electrolyte for redox flow batteries (RFBs) due to the advantages of high ionic conductivity, environmentally benign, safety and low cost. However, the underexplored redox properties of organic materials and the narrow thermodynamic electrolysis window of water (1.23 V) hinder their wide applications. Therefore, seeking suitable organic redox couples and aqueous electrolytes with a high output voltage is highly suggested for advancing the aqueous organic RFBs. In this work, the functionalized phenazine and nitroxyl radical with electron-donating and electron-withdrawing group exhibit redox potential of −0.88 V and 0.78 V vs. Ag, respectively, in "water-in-ionic liquid" supporting electrolytes. Raman spectra reveal that the activity of water is largely suppressed in "water-in-ionic liquid" due to the enhanced hydrogen bond interactions between ionic liquid and water, enabling an electrochemical stability window above 3 V. "Water-in-ionic liquid" supporting electrolytes help to shift redox potential of nitroxyl radical and enable the redox activity of functionalized phenazine. The assembled aqueous RFB allows a theoretical cell voltage of 1.66 V and shows a practical discharge voltage of 1.5 V in the "water-in-ionic liquid" electrolytes. Meanwhile, capacity retention of 99.91% per cycle is achieved over 500 charge/discharge cycles. A power density of 112 mW cm^{-2} is obtained at a current density of 30 mA cm^{-2}. This work highlights the importance of rationally combining supporting electrolytes and organic molecules to achieve high-voltage aqueous RFBs.

Keywords: Aqueous redox flow batteries; Water-in-ionic liquid electrolytes; High-voltage aqueous batteries; Organic redox-active materials

1. Introduction

Renewable energy sources such as wind and solar power are increasingly used for electricity generation. However, their intermittent features that are affected by weather and geographic conditions require efficient energy storage system to facilitate their integration into the grid network [1–3]. Redox flow batteries (RFBs) are considered as a promising technology for grid-scale stationary energy storage due to the merit of decoupled power and energy density, by storing redox electrolytes in exterior tanks [4]. Unlike other energy storage technologies, aqueous RFBs display unique advantages of fast charge/discharge response, good scalability, inherent safety and long lifetime [5,6]. The redox electrolytes, containing electro-active materials dissolved in supporting electrolytes, play an important role in electrochemical performance [7,8].

* Corresponding author.
E-mail addresses: zhifenghuang@xtu.edu.cn (Z. Huang), taoli@hnu.edu.cn (L. Tao), ruiyong.chen@liverpool.ac.uk (R. Chen).

https://doi.org/10.1016/j.gee.2022.09.005

In conventional inorganic all-vanadium RFBs, the redox reactions depend on the valence change of vanadium ions in both catholyte and anolyte, resulting in long-term cyclability without electrolyte cross-contamination [9–12]. However, the drawbacks of high electrolyte cost and toxicity of electrolytes cause concerns for large-scale applications. Recently, the research interest of redox-active materials has partially shifted from resource-limiting transition metal-based materials to organic materials, attributing to their natural abundance, diverse molecular structures, facile molecular modification, and relatively low cost [13–16]. To date, a large number of organic materials such as quinones [17], nitroxyl radicals [18], viologens [19], and metallic ferrocenes [20] have been widely studied in RFBs due to their tunable solubility, reversible redox reaction, and adjustable redox potential. Nevertheless, active organic materials-based RFBs still encounter several challenges. For instance, the organic compounds may undergo parasitic side reactions with the solvents and salts, resulting in insufficient chemical stability [21]. On the other hand, the supporting electrolytes show poor compatibility with redox materials in terms of ions mobility and electrochemical stability window. Typical organic solvents suffer from safety issues and insufficient ionic conductivity (<10 mS cm^{-1}), while aqueous electrolytes are restricted by their narrow operating voltage [22–24]. As a result, most reported aqueous RFBs have a cell voltage generally below 1.3 V. The development of high-voltage aqueous electrolytes utilizing redox-active organic materials is therefore highly desirable [25,26].

Ionic liquids, showing attractive physicochemical properties such as excellent thermal stability, wide electrochemical stability window (ESW), versatile structure, superior thermal stability and non-flammability, have been widely used in energy storage devices (e.g., lithium-ion batteries, supercapacitors, and RFBs, etc.) [27–31]. Certain ionic liquids have been regarded as potential electrolytes due to their broad ESW and flame-resistant features [32]. However, typical room-temperature ionic liquids with high viscosity and insufficient ionic conductivity resulted in a low operating current density during charge/discharge for RFBs and thus limited power performance [33]. As an alternative strategy, hydrophilic ionic liquids mixed with water can offer sufficient ionic conductivity without sacrificing too much of the ESW [34–36]. In addition, ionic liquids allow improved solubility and cycling stability of some organic electro-active materials due to enhanced interactions among different species [35,37]. Hence, hydrophilic ionic liquids-based aqueous electrolytes are promising towards high-performance aqueous RFBs.

Organic small molecules derived from natural phenazine (PZ) derivatives have demonstrated good reversible redox reactions at low negative potentials [38–41]. Organic nitroxyl radicals are well-known as stable species in catholyte for reversible electrochemical redox reactions in aqueous media [42]. In this work, a redox flow cell delivering a practical discharge voltage of 1.5 V was reported by using "water-in-ionic liquid" electrolytes, and by pairing an electron-donating group modified phenazine (showing a low negative potential of −0.88 V vs. Ag) as anolyte, and an electron-withdrawing group modified nitroxyl radical (showing a high positive potential of 0.78 V vs. Ag) as catholyte. Raman spectroscopic analysis revealed the stabilizing mechanism for suppressed water decomposition in the "water-in-ionic liquid" electrolytes, which assures the electroactivity of both redox-active organic materials to maximize the cell voltage. An energy efficiency of over 70% and capacity retention of over 99.91% per cycle at 30 mA cm^{-2} have been achieved for flow cell tests. A power density of up to 112 mW cm^{-2} was reached at ~100% state of charge (SOC). The results reported in this work are suggestive for developing sustainable, safe and high-performance next-generation aqueous RFBs.

2. Experimental details

2.1. Chemicals and preparation of electrolytes

2,3-diaminophenazine (DAPZ, >90%) and 4-hydroxy-2,2,6,6-tetramethylpiperidine 1-oxyl (4-HO-TEMPO, >98%) were purchased from Sigma−Aldrich. The studied ionic liquids of imidazolium (>99%), pyrrolidinium (>99%), and piperidinium (>99%) chlorides from Iolitec (Germany) were used without further purification. The synthesis and characterization of imidazolium-grafted TEMPO (Im-TEMPO) were reported previously [29]. The "water-in-ionic liquid" supporting electrolytes are described in terms of molality (m,mol kg^{-1}_{water}). For instance, 3 mmol 1-butyl-3-methylimidazolium chloride (BMImCl) or 1-ethyl-3-methylimidazolium chloride (EMImCl) was added in 1 g water to form a 3 mol L^{-1} BMImCl/H_2O, or a 3 mol L^{-1} EMImCl/H_2O, respectively. For the 10 mol L^{-1} BMImCl/H_2O, water accounts for about 38.3% of the volume fraction.

2.2. Characterization

The Raman spectroscopy (Ventana 532 nm, Ocean Optics) was used to study the molecular interactions of "water-in-ionic liquid" electrolytes with an acquisition time of 50 ms. To record the feature of pure ionic liquids, the ionic liquids were prepared in the Ar-filled glove box (<5 ppm, H_2O) and then sealed in the cuvette under Ar protection. The "water-in-ionic liquid" solutions of different molalities were loaded in the cuvette with a liquid volume of 5 mL.

Density functional theory (DFT) calculations were performed using Gaussian 09 program at the B3LYP/6-31 G(d, p) level [43]. For each optimized structure, their highest occupied molecular orbital (HOMO) and lowest unoccupied molecular orbital (LUMO) were analyzed by Gaussview 05.

2.3. Electrochemical measurements

2.3.1. Cyclic voltammetry (CV) measurements

The electrochemical measurements were conducted at the ambient atmosphere. A Bio-Logic VMP3 potentiostat was employed to conduct the electrochemical measurements. CV measurements were performed using a three-electrode system consisting of glassy carbon working electrode (1 mm

diameter), a Pt foil counter electrode, and a silver wire quasi-reference electrode. The working electrode was polished with sandpaper and rinsed with deionized water before the measurement. CV curves were recorded at different scan rates from 10 to 300 mV s^{-1} at room temperature.

2.3.2. Rotating disk electrode (RDE) measurements

Linear sweep voltammetry (LSV) experiments were conducted in 3 mol L^{-1} BMImCl/H_2O electrolyte with a three-electrode system consisting of a glassy carbon rotating disk working electrode (diameter of 5 mm), a Pt counter electrode, and Ag wire quasi-reference electrode. During the experiments, the working electrode was rotated from 300 to 1800 r min^{-1} with an increment of 300 r min^{-1} (PINE research instrument). Three scans at each rotation rate were collected to obtain the average value. LSV scans at a rate of 5 mV s^{-1} were conducted from 0.5 to 1.1 V vs. Ag for the catholyte (Im-TEMPO), and from −1.4 to −0.3 V vs. Ag for the anolyte (DAPZ). The mass transport controlled limiting current was recorded at 1.05 and −1.30 V vs. Ag for Im-TEMPO and DAPZ, respectively.

The diffusion coefficient (D) was determined from the slope of the Levich plot, limiting current (i_{lim}) *vs.* square root of the rotation rate ($\omega^{1/2}$, (rad s^{-1})$^{1/2}$), by using Equation (1),

$$i_{lim} = 0.62\ nFA\ \nu^{-1/6}\omega^{1/2}D^{2/3}\ C_0 \quad (1)$$

where n is the number of the electrons transferred, F is the Faraday constant (26.8 Ah mol^{-1}), A is the disk area (0.196 cm^2), C_0 is the bulk concentration of electroactive species (1×10^{-6} mol cm^{-3}), and ν is the kinematic viscosity, which has been determined to be 0.027 cm^2 s^{-1} for a 3 mol L^{-1} BMImCl/H_2O electrolyte [35].

In the LSV curve, before the limiting current is reached, the mass transfer independent kinetic current (i_k) at different overpotentials (η) was determined by using the Koutecký–Levich equation:

$$1/i_m = 1/i_k + 1/i_{mt} \quad (2)$$

by extrapolating the Koutecký–Levich plot ($1/i_m$ vs. $\omega^{-1/2}$) to infinite rotation rate, where i_m is the measured current, and i_{mt} is the mass transport current.

Tafel equation was applied to determine the exchange current (i_0) and charge transfer rate constant (k_0):

$$\log_{10}(i_k) = \log_{10}(i_0) + \alpha nF\eta/2.303RT \quad (3)$$

$$i_0 = nFAC_0k_0 \quad (4)$$

where n is the number of electrons in the rate-limiting step, α is the charge transfer coefficient, η is the overpotential (V), R is the universal gas constant (J K^{-1} mol^{-1}), T is the temperature (K).

2.3.3. Flow battery tests

A homemade flow cell with an active area of 4 cm^2 (2.0 cm × 2.0 cm) was used. The commercial Fumasep® FAA-3-30 anion exchange membrane (Fumatech, Germany) with a thickness of 30 μm was soaked in 1 mol L^{-1} KOH at 60 °C for 30 min and then immersed in 1 mol L^{-1} NaCl for 24 h at room temperature. The pre-treated membranes were stored in an aqueous imidazolium solution at room temperature before use and assembled in a cell in a wet form. The graphite felt (GFD4.6 EA, Sigracell® Carbon) was first immersed in 1 mol L^{-1} H_2SO_4 for 24 h and then thermally treated at 400 °C for 24 h in static air. The electrolytes containing DAPZ (20 mmol L^{-1}) and Im-TEMPO (42 mmol L^{-1}) in the supporting electrolytes were circulated by a peristaltic pump (ShenChen, China) at flow rates of 55 mL min^{-1}. The reservoirs were purged with Ar to reduce any O_2 in the system, then sealed with paraffin oil (Roth, Germany) as the top layer before the test. The volumetric energy density was calculated based on the electrolyte volume of the positive compartment (8 mL). The flow battery was charged and discharged galvanostatically at room temperature in the potential range between 0.6 and 2.2 V at varied current densities from 1.25 to 30 mA cm^{-2}. Electrochemical impedance spectroscopy (EIS) was performed at the open-circuit voltage, with a voltage perturbation of 5 mV, and a frequency ranging from 100 kHz to 10 mHz.

3. Results and discussion

For the assembly of high-voltage flow batteries, the redox-active materials with a large redox potential difference are expected. Thereof, the catholyte of TEMPO grafted with imidazolium group and anolyte of phenazine decorated with diamino moiety were paired to construct a redox flow battery in this work (Fig. 1a). The catholyte of Im-TEMPO could easily release one electron and be oxidized to an oxo-piperidinium cation. The DAPZ experienced a two-electron transition in the neutral aqueous electrolyte, as shown in Fig. 1b.

The energy levels of LUMO and accordingly the redox potentials can be shifted by introducing electron-withdrawing/-donating substituents to the 4-HO-TEMPO and phenazine (PZ), respectively. To evaluate the redox properties of these functionalized molecules, the energy levels of the LUMO and the HOMO/singly occupied molecular orbital (SOMO) were calculated using DFT. Fig. 1c shows that the LUMO of DAPZ (−1.92 eV) is higher than that of pristine phenazine (−2.30 eV), indicating a higher electron affinity and more negative reduction potential [44]. Meanwhile, the electron-withdrawing imidazolium substituent in TEMPO altered the energy level of the SOMO by 3.23 eV, leading to a positively shifted redox potential. In addition, the gap between the SOMO and LUMO levels for Im-TEMPO ($\Delta E = 2.47$ eV) was narrower than that of 4-HO-TEMPO (5.81 eV). A similar tendency for HOMO–LUMO energy gap was obtained for

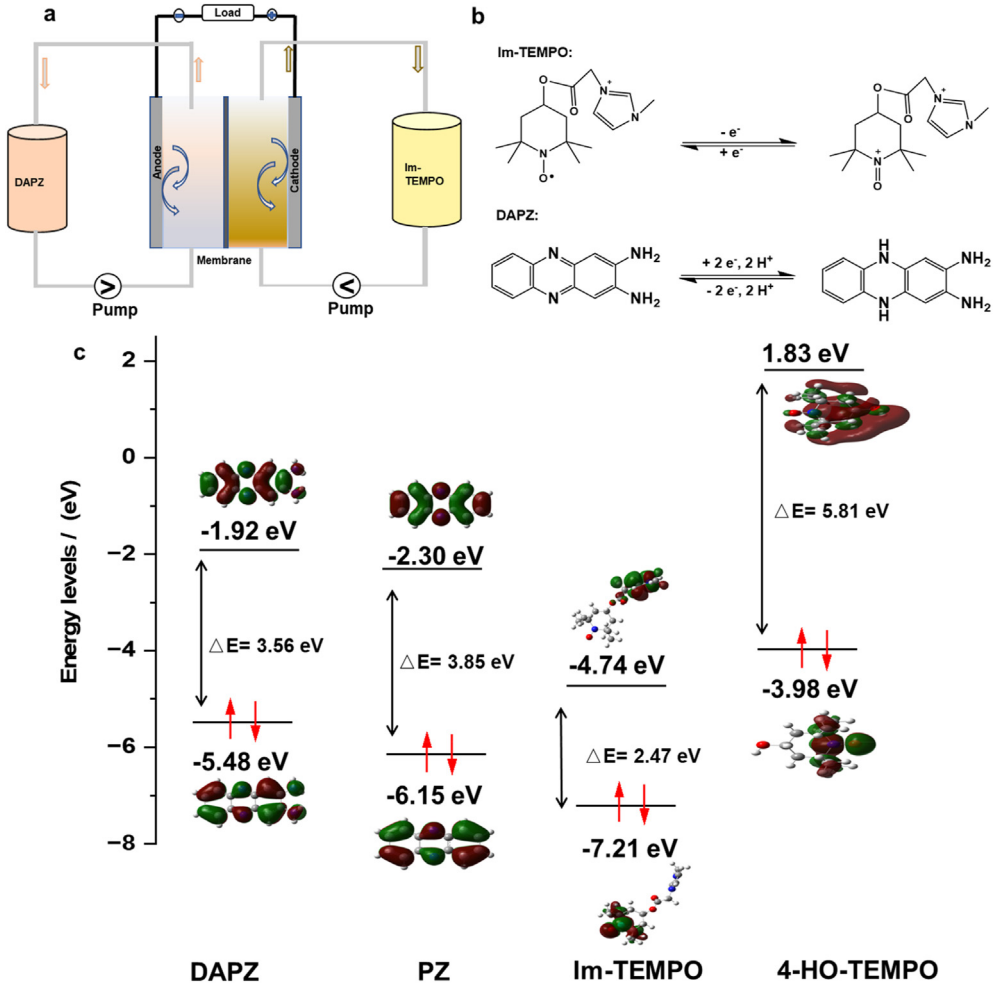

Fig. 1. (a) The schematic of a redox flow battery. (b) The half–cell reactions of the redox-active materials. (c) DFT-optimized structure and the relative energy levels of the frontier HOMO/SOMO and LUMO orbitals of the decorated molecules of Im-TEPMPO and DAPZ and pristine 4-HO-TEMPO and phenazine (PZ).

DAPZ (3.56 eV) and PZ (3.85 eV) as well. This indicates improved intrinsic electronic conductivity of the functionalized redox species compared to the unmodified 4-HO-TEMPO and PZ [45–47].

The stability windows of several "water-in-ionic liquid" electrolytes were investigated by CV measurements, as shown in Fig. 2a. Upon cathodic scan, the H_2 evolution reaction was noticeably suppressed in the 10 mol L^{-1} piperidinium-based and pyrrolidinium-based aqueous electrolytes, where the H_2 evolution occurred below −2.4 V vs. Ag. Upon anodic scan, the O_2 evolution was detected at 1.2 V vs. Ag, resulting in an overall wide ESW of about 3.6 V. This ESW is even wider than that (3 V) for a reported super-concentrated lithium bis(trifluoromethanesulfonyl)imide (LiTFSI) aqueous solution [48]. Our supporting electrolytes allow a better stability at more negative potentials, which is favorable for selecting a broad range of anolyte to maximize the overall cell voltage in an aqueous RFB. In the case of imidazolium-based electrolyte, a relatively narrower ESW was indicated due to the acidic feature of the imidazolium ring that shows reduction preference at the applied potentials [49]. Apparently, the observed ESW of aqueous electrolytes indicates a significant suppression of water splitting, considering the thermodynamic limit of water electrolytes (~1.23 V) [34]. Note that in contrast to other "water-in-ionic liquid" electrolytes, the imidazolium-based electrolyte exhibits a negligible current variation at about 0.9 V vs. Ag upon anodic scan, suggesting a better electrochemical stability. Therefore, the imidazolium-based ionic liquids were employed as supporting electrolytes for further studies, which also offered a sufficient stability window for the studied anolyte.

Raman spectra of neat water, neat BMImCl and imidazolium-based aqueous electrolytes with different molalities (3, 5, 10 and 20 mol L^{-1}) are shown in Fig. 2b. The liquid water showed an intense and broad band in the range of 3150–3450 cm^{-1}, which is attributed to −OH stretching modes. The most prominent stretching at around 3215 and 3420 cm^{-1} represented the symmetric and asymmetric O–H stretching vibration band, respectively [50]. With increasing imidazolium molality in water, the typical −OH stretching vibration at 3215 cm^{-1} distinctly vanished. This indicates that the strong hydrogen bonds of the free water molecules were significantly broken with formation of new hydrogen bond between the water and anions, leading to a reduced water activity [51–53].

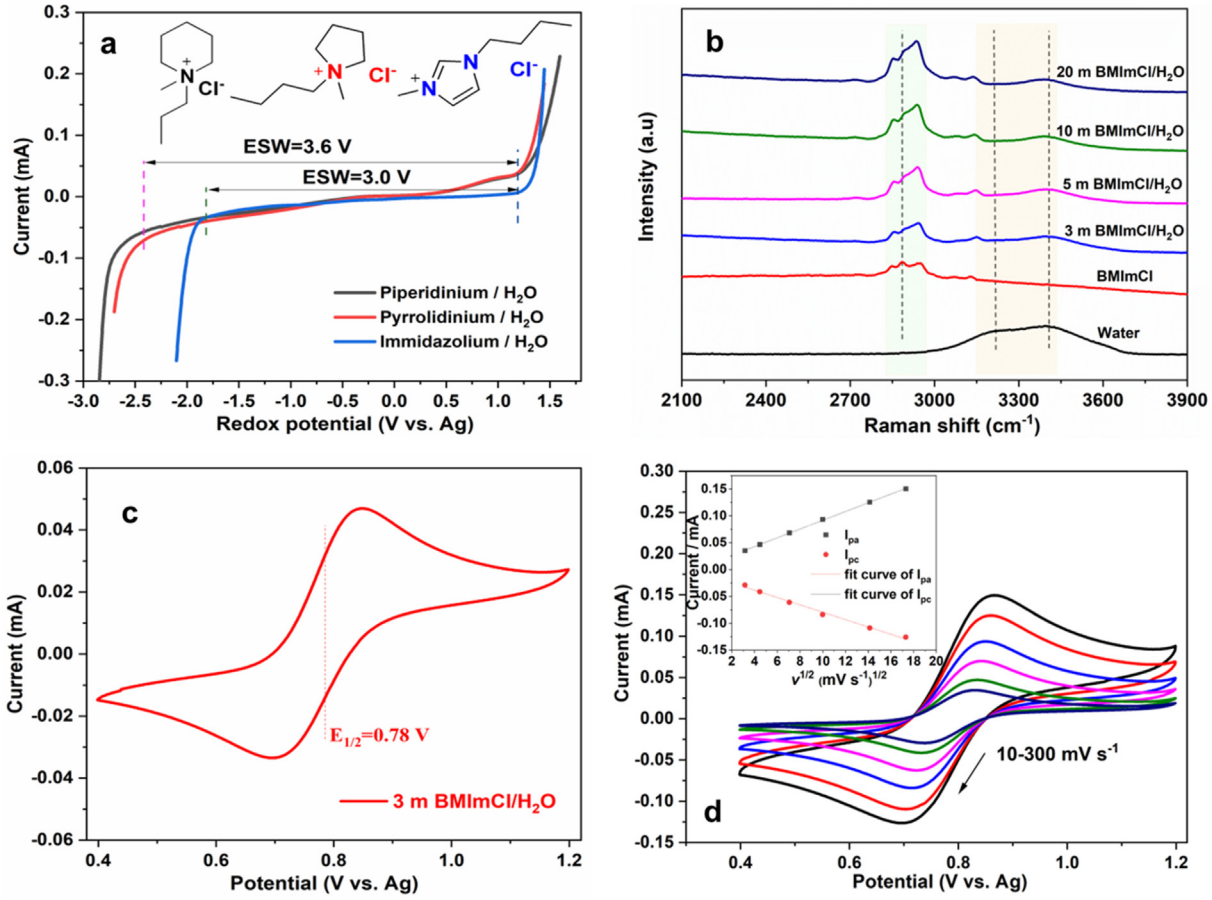

Fig. 2. (a) The ESW of three types of "water-in-ionic liquid" electrolytes at a molality of 10 mol L^{-1}. (b) Raman spectra of the "water-in-imidazolium chloride" electrolytes (3, 5, 10 and 20 mol L^{-1}), pure water, and pure imidazolium chloride. (c) Half potential ($E_{1/2}$) of 10 mmol L^{-1} Im-TEMPO in 3 mol L^{-1} BMImCl/H_2O supporting electrolyte at 50 mV s^{-1}. (d) CV curves 10 mmol L^{-1} Im-TEMPO in 3 mol L^{-1} BMImCl/H_2O electrolyte at varied scan rates from 10 to 300 mV s^{-1}. Inset: the anodic and cathodic peak current (i_p) vs. the square root of potential scan rate ($\nu^{1/2}$).

Raman peaks between 2830 and 3150 cm^{-1} can be assigned to the stretching vibration of C–H bonds of the imidazolium ring and aliphatic C–H bonds in pure BMImCl [54,55]. Note that the typical peak at 2885 cm^{-1} associated with the C2–H bond of the imidazolium ring is absent after adding water, indicating that the $BMIM^+$ cations participate in the formation of hydrogen bond with water [50,56,57]. In such case, the water molecules are trapped by the ionic liquids, leading to the formation of "water-in-ionic liquid" electrolytes. In consistent with the LSV results, the prepared electrolyte is promising for high cell voltage battery applications without causing water splitting.

Since the Raman features are similar between the 3 mol L^{-1} and 10 mol L^{-1} aqueous imidazolium chloride electrolytes, and higher ionic conductivity is expected in 3 mol L^{-1} electrolytes, next, 3 mol L^{-1} "water-in-ionic liquid" electrolytes were studied. We further confirmed that a wide ESW was observed for 3 mol L^{-1} BMImCl/H_2O (Fig. S1a). As shown in Fig. 2c, the measured half potential ($E_{1/2}$) of 0.78 V vs. Ag (or 0.87 V vs. Ag/AgCl, Fig. S1b) in 3 mol L^{-1} BMImCl/H_2O was observed for the Im-TEMPO with an electron-withdrawing group. This value is higher than the $E_{1/2}$ of unmodified 4-HO TEMPO measured either in 3 mol L^{-1} BMImCl/H_2O [34], or in conventional aqueous NaCl electrolyte [35]. It is considered that that molecular interactions play a critical role to govern the electrochemical properties of redox-active organic materials [34,57]. A strong ion-pairing in "water-in-ionic liquid" electrolyte is expected and responsible for the increased redox potential. The peak current versus the square root of the scan rate demonstrated a linear relationship, implying that Im-TEMPO underwent a typical diffusion-controlled reaction (Inset in Fig. 2d). Good compatibility between the Im-TEMPO and the supporting electrolyte can be confirmed, exhibiting steady electroactivity over 100 CV cycles (Fig. S2).

For the DAPZ anolyte, two $-NH_2$ groups were introduced to phenazine to downshift the redox potential, leading to two pairs of redox peaks with $E_{1/2}$ of −0.72 V and −0.88 V vs. Ag. Interestingly, two pairs of peaks instead of one are observed that is ascribed to the ion-pair effect between the reduced intermediate and the $BMIm^+$ cations [35]. The redox activity and reversibility of the DAPZ maintained over cycling (Fig. S3). In contrast, the DAPZ was electrochemically inactive in aqueous NaCl electrolyte (Fig. S4). Clearly, our "water-in-ionic liquid" electrolyte unlocked the redox chemistry of DAPZ as anolyte for aqueous RFBs. The hydrogen bonds play

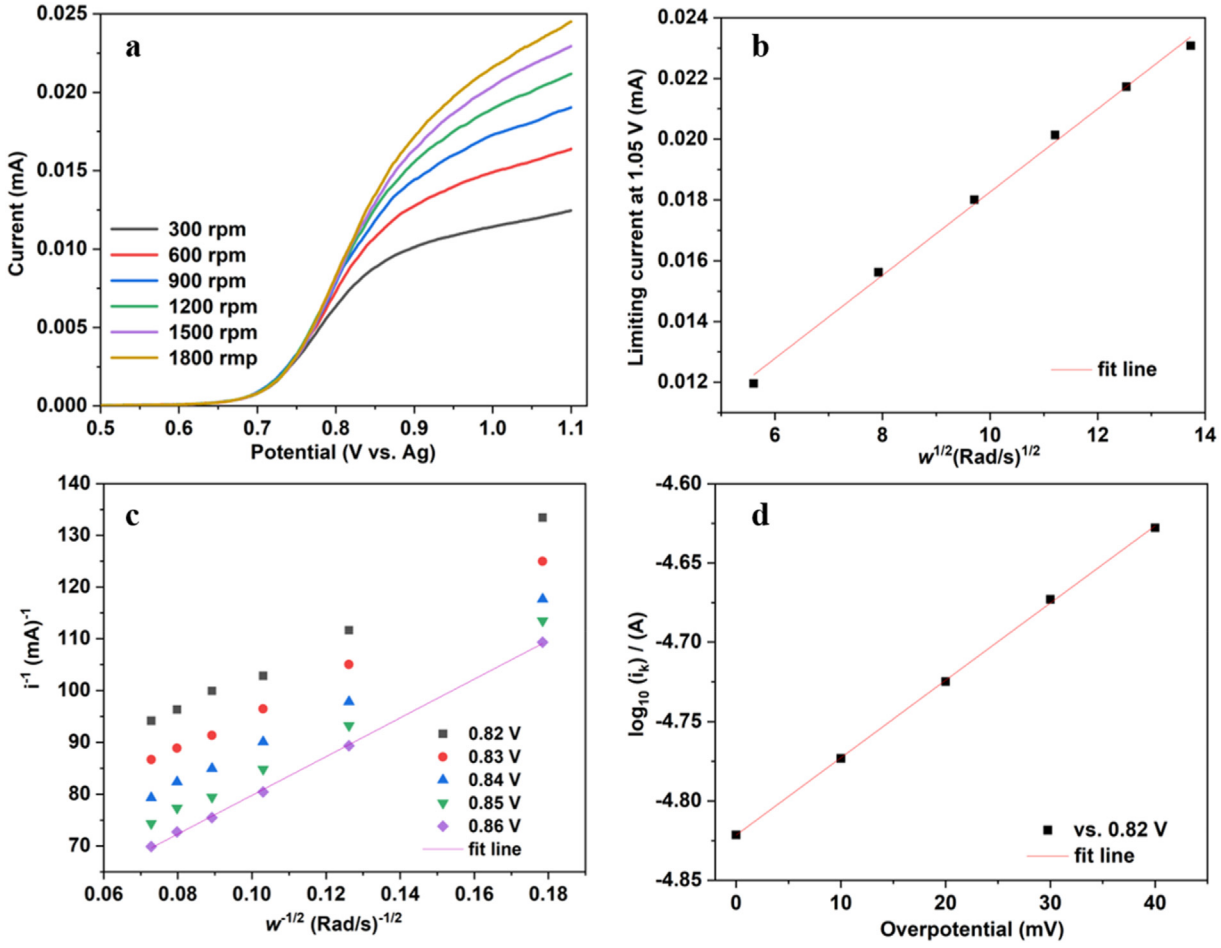

Fig. 3. RDE data and analysis for the catholyte of 1 mmol L^{-1} Im-TEMPO in 3 mol L^{-1} BMImCl/H_2O. (a) Current vs. potential at various rotating rates from 300 to 1800 r min^{-1} with a potential sweep rate of 5 mV s^{-1}. (b) Levich plot derived from (a) with the limiting current collected at 1.05 V vs. Ag. (c) Koutecký–Levich plot derived from (a) at different potentials vs. Ag. (d) Tafel plot.

a critical role on the molecular reactivity, which can be controlled by a rational design of the electrolyte formulation. Through ion-pairing effect, the ionic liquid can stabilize the reduced form of the DAPZ [58]. The partial trapping of water molecules in the "water-in-ionic liquid" electrolyte reduced the occurrence of side reactions between DAPZ and water. For the DAPZ, a solubility of 0.1 mol L^{-1} was reached in the "water-in-ionic liquid" electrolytes until no further materials can be dissolved anymore in the electrolytes.

To quantify the electrochemical reaction kinetics of redox species in 3 mol L^{-1} BMImCl/H_2O electrolytes, LSV measurements were carried out using a RDE electrode, as shown in Fig. 3. The LSV curves for Im-TEMPO reveal that the mass transport-controlled limiting current (i_{lim}) increased with rotation rates (ω) in the range of 300–1800 r min^{-1} (Fig. 3a). From the linear fitting of the Levich plots (i_{lim} vs. $\omega^{1/2}$), the diffusion coefficient (D_i) of the catholyte was calculated to be 4.62×10^{-7} cm^2 s^{-1} (Fig. 3b). The k_0 during the oxidation process was calculated to be 7.98×10^{-4} cm s^{-1}, from the Koutecký–Levich plot ($1/i_m$ vs. $\omega^{-1/2}$) (Fig. 3c) and Tafel plot ($\log_{10}(i_k)$ vs. η) (Fig. 3d), which is two orders of magnitude larger than the value (2.8×10^{-6} cm s^{-1} for VO^{2+}/VO_2^+ [58]) reported for the acidic vanadium electrolyte. Moreover, the stepwise two-electron transition reaction was observed in the range of −1.2 to −1.0 V vs. Ag, which is consistent with the CV results. The related D_i and k_0 of DAPZ anolyte were 1.12×10^{-6} cm^2 s^{-1} and 4.91×10^{-2} cm s^{-1}, respectively (Fig. S5). Regarding the high diffusion coefficients for both DAPZ and Im-TEMPO in 3 mol L^{-1} BMImCl/H_2O, they are favorable to reduce the cell voltage loss caused by mass transport and to enhance rate performance in a flow cell.

The electrochemical charge/discharge cycling performance of the DAPZ anolyte and Im-TEMPO catholyte in 3 mol L^{-1} BMImCl/H_2O electrolytes was then investigated in a redox flow battery with a cut-off voltage of 2.2 V. As shown in Fig. 4a, the DAPZ displayed a more negative redox potential of −0.88 V vs. Ag, and Im-TEMPO presented a positive redox potential of 0.78 V vs. Ag, leading to a theoretical cell voltage of 1.66 V. Noticeably, the obtained theoretical cell voltage of 1.66 V is among the highest of the reported aqueous RBFs using all-organic redox couples (Fig. 4b). Due to the two-electron transfer feature of the DAPZ anolyte, the charge/discharge voltage profile of the DAPZ/TEMPO cell exhibited two well-defined plateaus (Fig. 4c), indicating that the anolyte

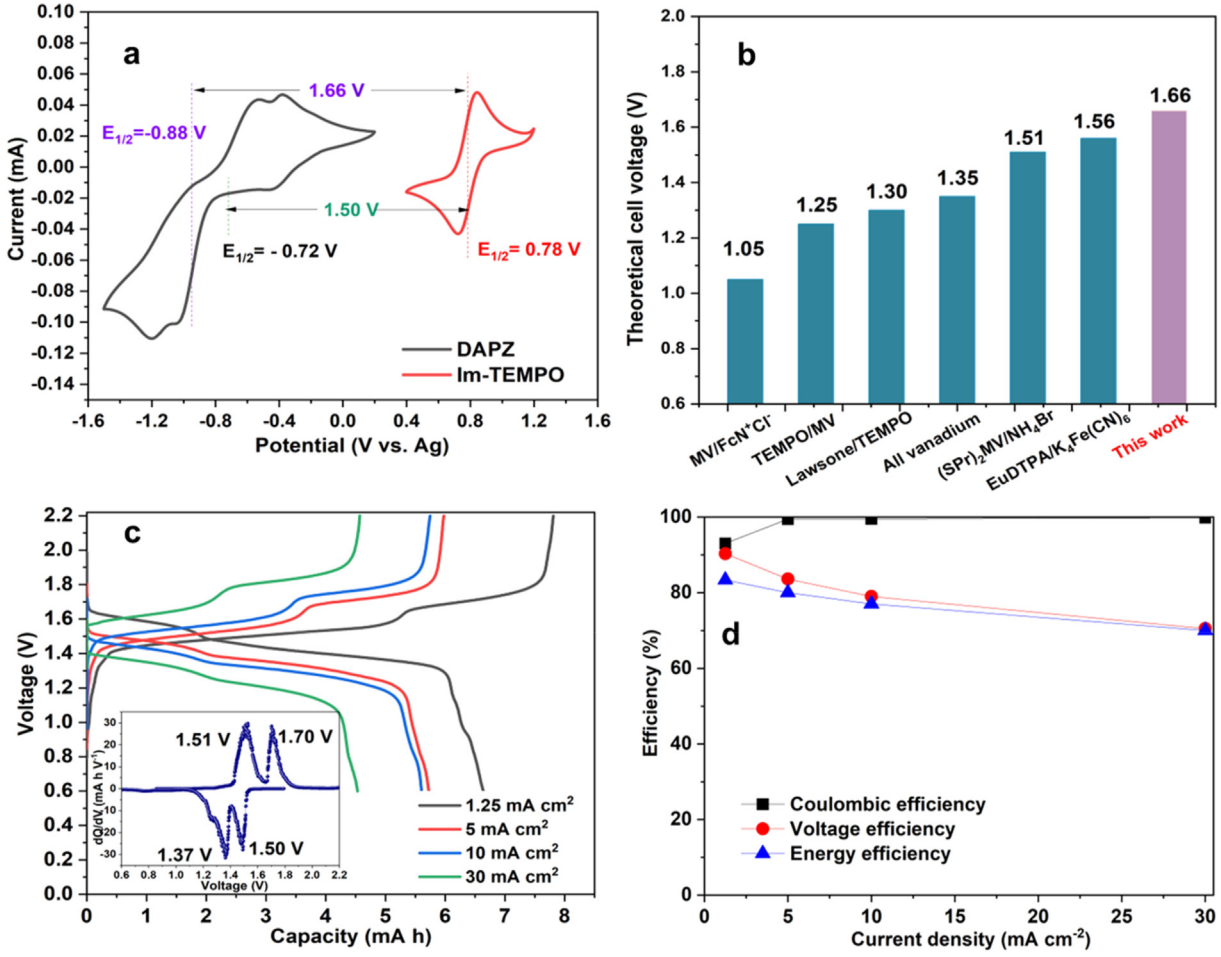

Fig. 4. (a) CV curves 0.01 mol L^{-1} DAPZ and Im-TEMPO in 3 mol L^{-1} BMImCl/H_2O electrolyte at 50 mV s^{-1}. The electrochemical performance of 0.02 mol L^{-1} DAPZ and 0.042 mol L^{-1} Im-TEMPO aqueous RFBs in 3 mol L^{-1} BMImCl/H_2O supporting electrolyte. (b) Comparision of theoretical cell voltages of recently reported aqueous RFBs, combining all-organic materials and hybrid organic/inorganic redox couples [19,59–63]. MV: methyl viologen [19], FcN^+Cl^-: (ferrocenylmethyl)trimethylammonium chloride [19], Lawsone: 2-hydroxy-1,4-naphthoquinone [61], $(SPr)_2MV$: 1,10-bis(3-sulfonatopropyl)-4,40-bipyridinium [63], EuDTPA: europium diethylene-triaminepentaacetic acid [62]. (c) Voltage profiles at different current densities. Inset shows the dQ/dV profile derived from the charge/discharge curves at the current density of 1.25 mA cm^{-2}. (d) The corresponding cycling efficiencies.

and catholyte underwent reversible redox reactions. The cell cycled at a current density of 1.25 mA cm^{-2} showed a relatively higher discharge cell voltage due to its relatively lower ohmic loss. Inset in Fig. 4c shows clearly the two pairs of redox events at 1.70 V/1.50 V and 1.51 V/1.37 V, in good agreement with the CV results. Noticeably, the high charge cut-off voltage of 2.2 V did not cause gas evolution from water electrolysis, demonstrating the excellent stability of applied "water-in-ionic liquid" electrolytes. A high discharge voltage of 1.50 V and 1.37 V was obtained at the current density of 1.25 and 30 mA cm^{-2}, respectively. The displayed discharge voltage of 1.50 V is also regarded as one of the highest results in comparison with other aqueous RFBs (Table S1) [19,59–65]. The initially charged capacity was 8.4 mAh at a current density of 1.25 mA cm^{-2} at the first cycle, corresponding to 95.7% of capacity utilization. The discharge capacities were approximately 6.6, 5.8, 5.6 and 4.5 mAh, at current densities of 1.25, 5, 10 and 30 mA cm^{-2}, respectively. Fig. 4d shows the dependence of cycling efficiencies on the applied current densities between 1.5 and 30 mA cm^{-2}. At a current density of 1.5 mA cm^{-2}, the average Coulombic, voltage and energy efficiencies were 93%, 91% and 85%, respectively. As the current density increases, the Coulombic efficiency showed a gradual increase and eventually stabilized at about 99.8%, indicating the excellent reversibility of both catholyte and anolyte. At a current density of 30 mA cm^{-2}, a reduced voltage efficiency of 70% and an energy efficiency of 70% were observed due to the increased activation and ohmic polarization. These are, however, still comparable to that (70%) for a reported 4-trimethylammonium-TEMPO in aqueous NaCl electrolyte [66].

The cycling stability was further studied by operating the flow battery at 30 mA cm^{-2} for 500 cycles. Fig. 5a shows that the cell delivered a stable capacity of 4.5 mAh, corresponding to 53% of the theoretical capacity. The capacity dropped during the initial 10 cycles which may be related to the initial dissolved O_2 residual in the electrolyte or the possible interactions of redox species with the membrane. A good capacity retention

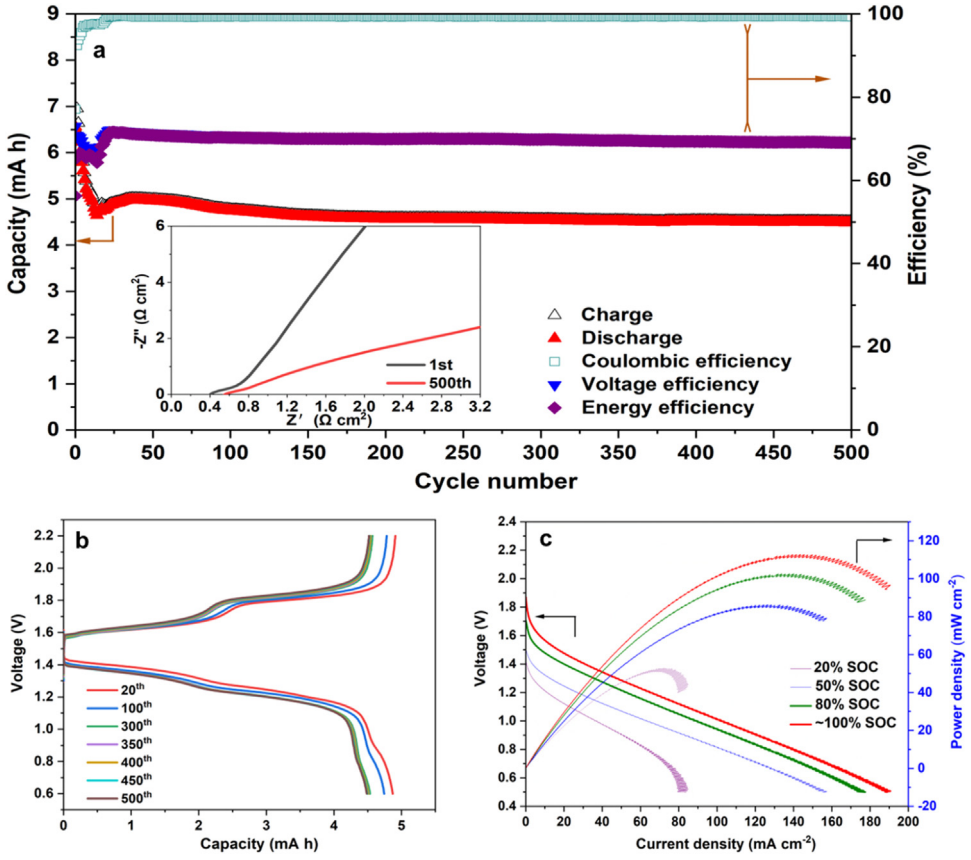

Fig. 5. The performance of aqueous RFBs with 20 mmol L^{-1} DAPZ and 42 mmol L^{-1} Im-TEMPO in 3 mol L^{-1} BMImCl/H_2O supporting electrolyte as anolyte and catholyte, respectively. (a) Capacity retention and cycling efficiencies over 500 cycles at 30 mA cm^{-2}. Inset shows the EIS of a flow battery at the 1st and 500th cycles. (b) Voltage profiles over 500 cycles at 30 mA cm^{-2}. (c) Polarization curves and power density at different SOC.

of 99.91% per cycle (or a capacity fate rate of 0.28% per day) and a high Coulombic efficiency approaching 99.9% were observed, implying an excellent chemical and electrochemical stability of the studied species. It is considered that the aqueous imidazolium chloride as reaction media enables a wide electrochemical stability window that prevents the water from splitting in the charge–discharge process and ultimately inhibits the unfavorable parasitic side reaction. EIS spectra (Inset in Fig. 5a) showed a small area resistance of 0.5 Ω cm^2 after 500 cycles, which was a slight increase in comparison with that of 0.36 Ω cm^2 at the initial state. This indicates that the membrane was chemically stable with well-remained ion pathway and has good compatibility with the electrolyte. Noticeably, the two distinct charge/discharge profiles maintained well over 500 cycles in Fig. 5b, indicating the excellent reversibility and stability of the studied organic compounds in the "water-in-ionic liquid" electrolyte. Post-cycling analysis was conducted to investigate the chemical stability of redox-active species. As shown in Fig. S6, no typical redox peaks from possible catholyte and anolyte crossover can be found at each side, suggesting a low level of cross-contamination of the redox species. The irreversible reduction at the low negative potential for the catholyte is relevant to the TEMPO-based catholyte. Meanwhile, the DAPZ and Im-TEMPO remained the two successive one-electron and one-electron transfer behavior, respectively, implying the high stability of the electrolyte. Fig. 5c shows the power density profiles of the flow cell at different SOC. The cell showed a peak power output of 80 mW cm^{-2} at 50% SOC. At near 100% SOC, the power output increased up to 112 mW cm^{-2}. The observed result is among the highest power densities reported so far for neutral aqueous organic RFBs [67].

4. Conclusions

In summary, we report a high-voltage aqueous redox flow battery by pairing electron-donating group modified phenazine (DAPZ) with electron-withdrawing group decorated TEMPO in "water-in-ionic liquid" electrolyte. The Raman spectroscopy revealed that ionic liquids interacted with water to suppress the water splitting, and thus provided a wide electrochemical stability window. In the demonstrated RFB cell, a discharge voltage of 1.5 V was validated in 3 mol L^{-1} BMImCl/H_2O electrolyte. A good capacity retention rate of 99.91% per cycle

was achieved over 500 cycles, showing good compatibility between the organic electro-active materials and the supporting electrolyte. This study provides a possible way for designing high-voltage and sustainable aqueous RFBs. The "water-in-ionic liquid" supporting electrolyte enabled the electrochemical redox activity of the DAPZ anolyte, as has been also found in a hydroquinone derivative catholyte [68]. The solubility of DAPZ anolyte is insufficient and future molecular engineering is needed to improve the solubility of redox species. Note that the present DAPZ anolyte was only tested down to −1.5 V vs. Ag. Our "water-in-ionic liquid" electrolytes allow a lower potential boundary of −2.5 V vs. Ag. There is great potential to explore new anolyte with lower negative potential to maximize the cell voltage of aqueous RFBs (>2V).

Conflict of interest

The authors declare that they have no known competing financial interests or personal relationships that could have appeared to influence the work reported in this paper.

Acknowledgements

Z.H. acknowledges the support from China Postdoctoral Science Foundation (Grant No. 2021M690960) and China CSC abroad studying fellowship. R.C. thanks the KIST Europe basic research funding "new electrolytes for redox flow batteries" and the partial financial support from the CMBlu Energy AG. Y.Z. thanks to the support received from the National Natural Science Foundation of China (Grant No. 22002009) and the Natural Science Foundation of Hunan Province (Grant No. 2021JJ40565).

Appendix A. Supplementary data

Supplementary data to this article can be found online at https://doi.org/10.1016/j.gee.2022.09.005.

References

[1] W. Wang, Q. Luo, B. Li, X. Wei, L. Li, Z. Yang, Adv. Funct. Mater. 23 (2013) 970–986.
[2] J. Noack, N. Roznyatovskaya, T. Herr, P. Fischer, Angew. Chem., Int. Ed. 54 (2015) 9776–9809.
[3] G.L. Soloveichik, Chem. Rev. 115 (2015) 11533–11558.
[4] R. Chen, Curr. Opin. Electrochem. 21 (2020) 40–45.
[5] D. Larcher, J.-M. Tarascon, Nat. Chem. 7 (2015) 19–29.
[6] R. Ye, D. Henkensmeier, S.J. Yoon, Z. Huang, D.K. Kim, Z. Chang, S. Kim, R. Chen, J. Electrochem. Energy Conver. Stor. 15 (2018) 010801.
[7] A.Z. Weber, M.M. Mench, J.P. Meyers, P.N. Ross, J.T. Gostick, Q. Liu, J. Appl. Electrochem. 41 (2011) 1137–1164.
[8] M. Skyllas-Kazacos, L. Cao, M. Kazacos, N. Kausar, A. Mousa, ChemSusChem 9 (2016) 1521–1543.
[9] S. Roe, C. Menictas, M. Skyllas-Kazacos, J. Electrochem. Soc. 163 (2016) A5023–A5028.
[10] W. Lee, M. Jung, D. Serhiichuk, C. Noh, G. Gupta, C. Harms, Y. Kwon, D. Henkensmeier, J. Membr. Sci. 591 (2019) 117333.
[11] H. Yoo, D. Lee, J.H. Kim, Green Energy Environ. 7 (2022) 704–711.
[12] L. Dai, K. Huang, Y. Xia, Z. Xu, Green Energy Environ. 6 (2021) 193–211.
[13] Z. Li, Y.-C. Lu, Chem 4 (2018) 2020–2021.
[14] Y. Ding, C. Zhang, L. Zhang, Y. Zhou, G. Yu, Chem. Soc. Rev. 47 (2018) 69–103.
[15] T.B. Schon, B.T. McAllister, P.-F. Li, D.S. Seferos, Chem. Soc. Rev. 45 (2016) 6345–6404.
[16] Q. Chen, Y. Lv, Z. Yuan, X. Li, G. Yu, Z. Yang, T. Xu, Adv. Funct. Mater. 32 (2022) 2108777.
[17] R. Feng, X. Zhang, V. Murugesan, A. Hollas, Y. Chen, Y. Shao, E. Walter, N.P. Wellala, L. Yan, K.M. Rosso, Science 372 (2021) 836–840.
[18] T. Janoschka, N. Martin, U. Martin, C. Friebe, S. Morgenstern, H. Hiller, M.D. Hager, U.S. Schubert, Nature 527 (2015) 78–81.
[19] B. Hu, C. DeBruler, Z. Rhodes, T.L. Liu, J. Am. Chem. Soc. 139 (2017) 1207–1214.
[20] Y. Zhao, Y. Ding, J. Song, G. Li, G. Dong, J.B. Goodenough, G. Yu, Angew. Chem., Int. Ed. 53 (2014) 11036–11040.
[21] X. Wei, W. Xu, J. Huang, L. Zhang, E. Walter, C. Lawrence, M. Vijayakumar, W.A. Henderson, T. Liu, L. Cosimbescu, Angew. Chem., Int. Ed. 54 (2015) 8684–8687.
[22] K. Gong, Q. Fang, S. Gu, S.F.Y. Li, Y. Yan, Energy Environ. Sci. 8 (2015) 3515–3530.
[23] D.D.P. Eugene, S. Beh, Rebecca L. Gracia, Kay T. Xia, Roy G. Gordon, Michael J. Aziz, ACS Energy Lett. 2 (2017) 639–644.
[24] X. Luo, W. Peng, Y. Li, F. Zhang, X. Fan, Green Energy Environ. 7 (2022) 858–899.
[25] K. Xu, Chem. Rev. 104 (2004) 4303–4418.
[26] M.L. Perry, K.E. Rodby, F.R. Brushett, ACS Energy Lett. 7 (2022) 659–667.
[27] E. Mourad, L. Coustan, P. Lannelongue, D. Zigah, A. Mehdi, A. Vioux, S.A. Freunberger, F. Favier, O. Fontaine, Nat. Mater. 16 (2017) 446–453.
[28] D.R. MacFarlane, N. Tachikawa, M. Forsyth, J.M. Pringle, P.C. Howlett, G.D. Elliott, J.H. Davis, M. Watanabe, P. Simon, C.A. Angell, Energy Environ. Sci. 7 (2014) 232–250.
[29] Z. Chang, D. Henkensmeier, R. Chen, J. Power Sources 418 (2019) 11–16.
[30] Z. Lei, B. Chen, Y.-M. Koo, D.R. MacFarlane, Chem. Rev. 117 (2017) 6633–6635.
[31] A. Tatlisu, Z. Huang, R. Chen, ChemSusChem 11 (2018) 3899–3904.
[32] M. Galiński, A. Lewandowski, I. Stępniak, Electrochim. Acta 51 (2006) 5567–5580.
[33] M. Watanabe, M.L. Thomas, S. Zhang, K. Ueno, T. Yasuda, K. Dokko, Chem. Rev. 117 (2017) 7190–7239.
[34] Z. Huang, P. Zhang, X. Gao, D. Henkensmeier, S. Passerini, R. Chen, ACS Appl. Energy Mater. 2 (2019) 3773–3779.
[35] Z. Huang, C.W. Kay, B. Kuttich, D. Rauber, T. Kraus, H. Li, S. Kim, R. Chen, Nano Energy 69 (2020) 104464.
[36] C.E. Bernardes, M.E. Minas da Piedade, J.N. Canongia Lopes, J. Phys. Chem. B 115 (2011) 2067–2074.
[37] Z. Huang, J. Lee, D. Henkensmeier, R. Hempelmann, S. Kim, R. Chen, J. Electrochem. Soc. 167 (2020) 160502.
[38] C. Wang, X. Li, B. Yu, Y. Wang, Z. Yang, H. Wang, H. Lin, J. Ma, G. Li, Z. Jin, ACS Energy Lett. 5 (2020) 411–417.
[39] G. Kwon, S. Lee, J. Hwang, H.-S. Shim, B. Lee, M.H. Lee, Y. Ko, S.-K. Jung, K. Ku, J. Hong, Joule 2 (2018) 1771–1782.
[40] A. Orita, M.G. Verde, M. Sakai, Y.S. Meng, Nat. Commun. 7 (2016) 13230.
[41] A. Hollas, X. Wei, V. Murugesan, Z. Nie, B. Li, D. Reed, J. Liu, V. Sprenkle, W. Wang, Nat. Energy 3 (2018) 508.
[42] X. Wei, W. Xu, M. Vijayakumar, L. Cosimbescu, T. Liu, V. Sprenkle, W. Wang, Adv. Mater. 26 (2014) 7649–7653.

[43] R.A. Gaussian09, Inc., Wallingford CT 121 (2009) 150–166.
[44] M. Huang, S. Hu, X. Yuan, J. Huang, W. Li, Z. Xiang, Z. Fu, Z. Liang, Adv. Funct. Mater. 32 (2022) 2111744.
[45] Y. Liu, Y. Li, P. Zuo, Q. Chen, G. Tang, P. Sun, Z. Yang, T. Xu, ChemSusChem 13 (2020) 2245–2249.
[46] Q. Chen, Y. Li, Y. Liu, P. Sun, Z. Yang, T. Xu, ChemSusChem 14 (2021) 1295–1301.
[47] C. Zhang, Z. Niu, S. Peng, Y. Ding, L. Zhang, X. Guo, Y. Zhao, G. Yu, Adv. Mater. 31 (2019) 1901052.
[48] L. Suo, O. Borodin, T. Gao, M. Olguin, J. Ho, X. Fan, C. Luo, C. Wang, K. Xu, Science 350 (2015) 938–943.
[49] P. Wasserscheid, T. Welton, John Wiley & Sons, 2008.
[50] R. Holomb, A. Martinelli, I. Albinsson, J.-C. Lassegues, P. Johansson, P. Jacobsson, J. Raman Spectrosc. 39 (2008) 793–805.
[51] J.G. McDaniel, A. Verma, J. Phys. Chem. B 123 (2019) 5343–5356.
[52] R. Yang, Y. Zhang, K. Takechi, E.J. Maginn, J. Phys. Chem. C 122 (2018) 13815–13826.
[53] K. Dong, S. Zhang, J. Wang, Chem. Commun. 52 (2016) 6744–6764.
[54] M. Becker, D. Rentsch, D. Reber, A. Aribia, C. Battaglia, R.S. Kühnel, Angew. Chem., Int. Ed. 60 (2021) 14100–14108.
[55] J. Meng, M. Ye, Y. Wang, Y. Sun, X. Zhang, K. Shi, X. Yan, Sci. China Chem. 65 (2022) 96.
[56] B. Fazio, A. Triolo, G. Di Marco, J. Raman Spectrosc. 39 (2008) 233–237.
[57] N.R. Dhumal, M.P. Singh, J.A. Anderson, J. Kiefer, H.J. Kim, J. Phys. Chem. C 120 (2016) 3295–3304.
[58] T. Yamamura, N. Watanabe, T. Yano, Y. Shiokawa, J. Electrochem. Soc. 152 (2005) A830–A836.
[59] L. Li, S. Kim, W. Wang, M. Vijayakumar, Z. Nie, B. Chen, J. Zhang, G. Xia, J. Hu, G. Graff, Adv. Energy Mater. 1 (2011) 394–400.
[60] T. Liu, X. Wei, Z. Nie, V. Sprenkle, W. Wang, Adv. Energy Mater. 6 (2016) 1501449.
[61] P. Hu, H. Lan, X. Wang, Y. Yang, X. Liu, H. Wang, L. Guo, Energy Storage Mater. 19 (2019) 62–68.
[62] P. Sun, Y. Liu, P. Zuo, Y. Li, Q. Chen, Z. Yang, T. Xu, J. Energy Chem. 60 (2021) 368–375.
[63] J. Luo, W. Wu, C. Debruler, B. Hu, M. Hu, T.L. Liu, J. Mater. Chem. A 7 (2019) 9130–9136.
[64] S. Pang, X. Wang, P. Wang, Y. Ji, Angew. Chem., Int. Ed. 60 (2021) 5289–5298.
[65] W. Liu, Z. Zhao, T. Li, S. Li, H. Zhang, X. Li, Sci. Bull. 66 (2021) 457–463.
[66] J. Luo, B. Hu, C. Debruler, T.L. Liu, Angew. Chem., Int. Ed. 57 (2018) 231–235.
[67] C. DeBruler, B. Hu, J. Moss, X. Liu, J. Luo, Y. Sun, T.L. Liu, Chem 3 (2017) 961–978.
[68] R. Ye, D. Henkensmeier, R. Chen, Sustain. Energy Fuels 4 (2020) 2998–3005.